Supporting Information

In-situ characterization reveals a favorable reconstruction of $BiVO_4$ in thermal catalysis

Cheng Chen[1,2#], Yifan Xu[3#], Chunyan Ma[1,2#], Bolei Chen[1,2], Fanglan Geng,[2] Xiaozhi Liu[4]*, Maoyong Song[1,2]*, and Guibin Jiang[2]

[1]Key Laboratory of Environmental Nanotechnology and Health Effects, Research Center for Eco-Environmental Sciences, Chinese Academy of Sciences, Beijing 100085, China

[2]State Key Laboratory of Environmental Chemistry and Ecotoxicology, Research Center for Eco-Environmental Sciences, Chinese Academy of Sciences, Beijing 100085, China

[3]Nanjing Institute of Environmental Sciences, Ministry of Ecology and Environment of China, Nanjing, 210042, China

[4]Beijing National Laboratory for Condensed Matter Physics, Institute of Physics, Chinese Academy of Sciences, Beijing, 100190, China

[#]Cheng Chen, Yifan Xu, and Chunyan Ma contributed equally to this work.

*Correspondence: liuxz@iphy.ac.cn; smsong@rcees.ac.cn

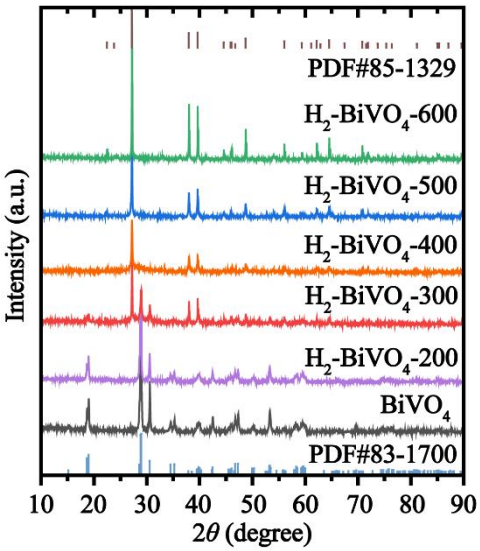

Figure S1. XRD characterization of the $BiVO_4$ and H_2-$BiVO_4$.

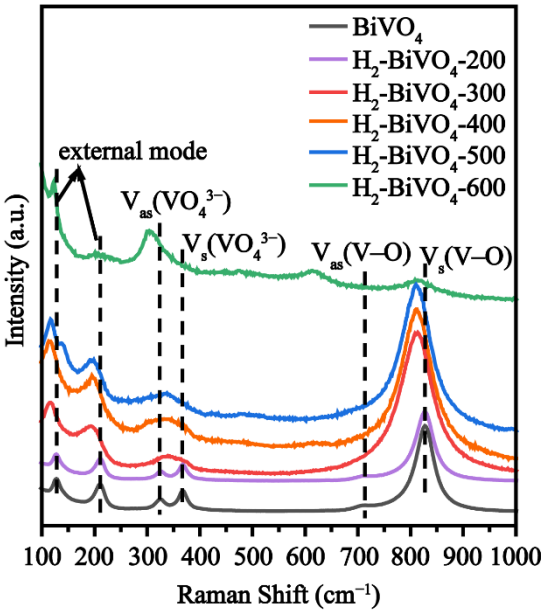

Figure S2. Raman characterization of the $BiVO_4$ and H_2-$BiVO_4$.

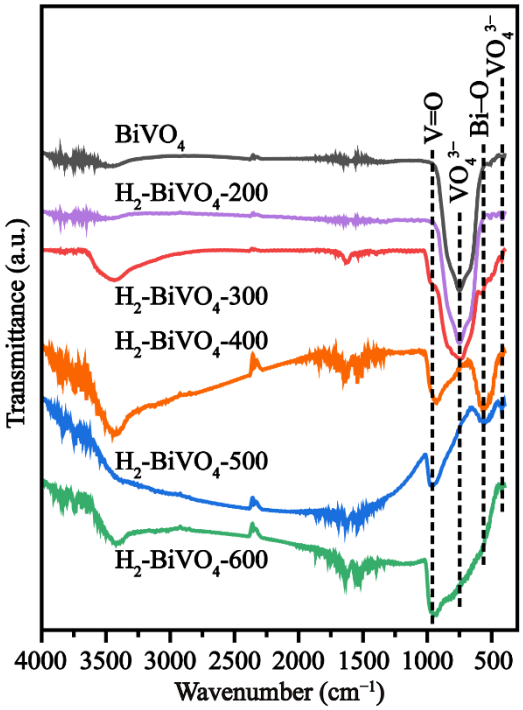

Figure S3. FTIR spectra of the $BiVO_4$ and H_2-$BiVO_4$.

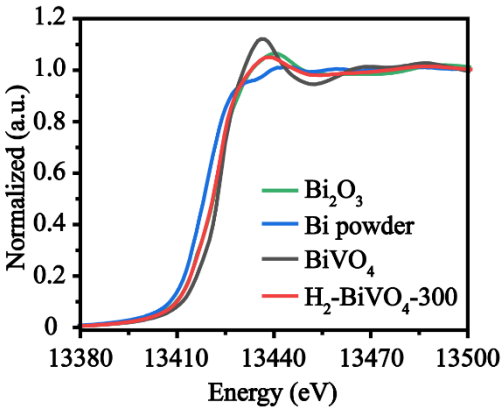

Figure S4. Bi L_3-edge XANES spectra of Bi powder, Bi_2O_3, $BiVO_4$, and H_2-$BiVO_4$-300, respectively.

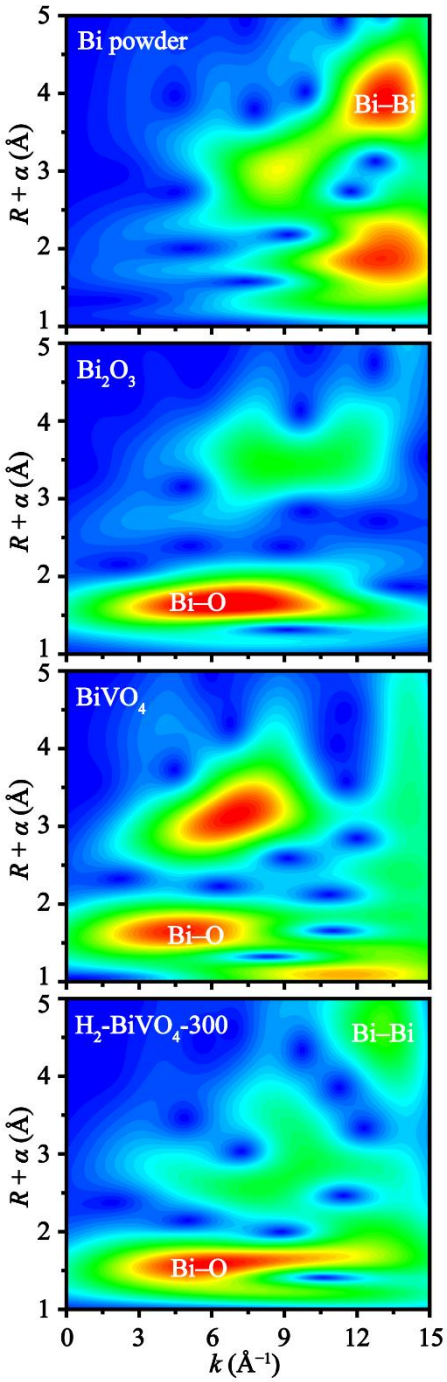

Figure S5. WT-EXAFS plots of Bi powder, Bi_2O_3, $BiVO_4$, and H_2-$BiVO_4$-300, respectively.

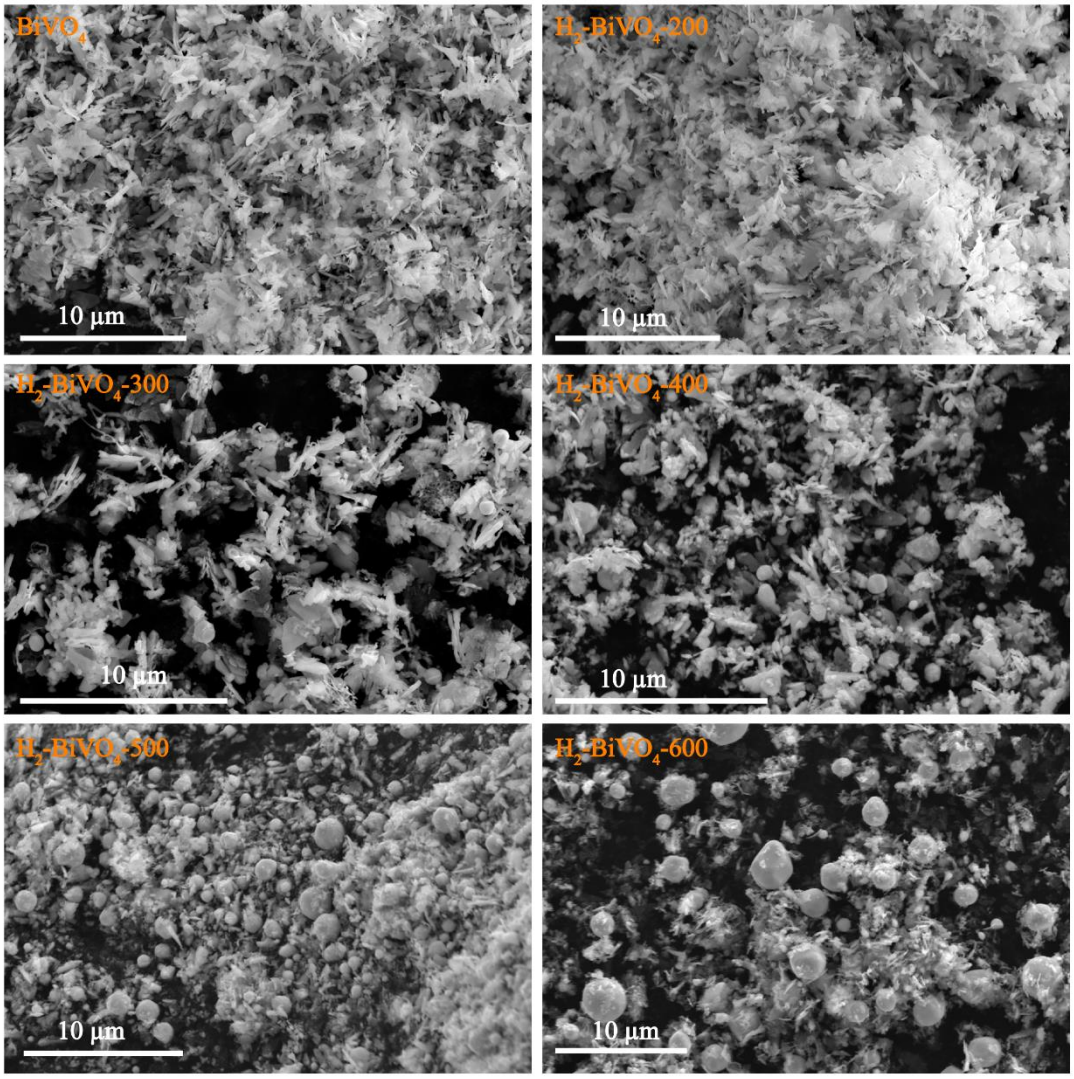

Figure S6. SEM images of the $BiVO_4$ and H_2-$BiVO_4$.

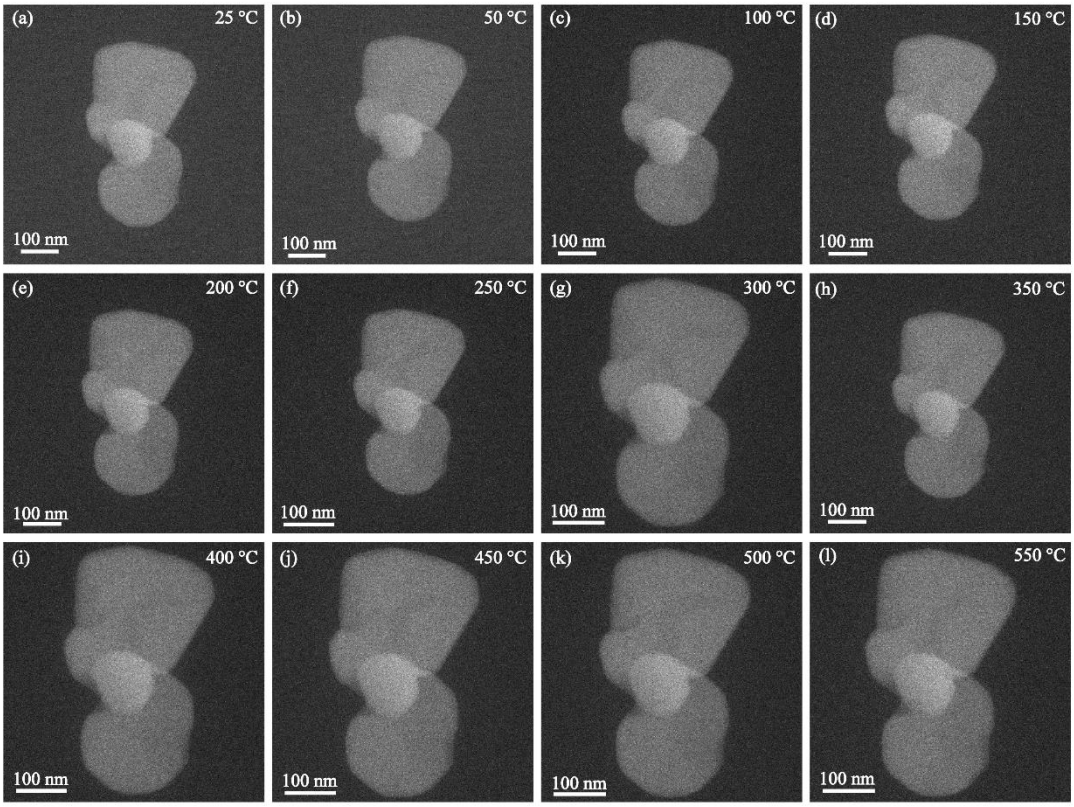

Figure S7. *In-situ* STEM images of the $BiVO_4$ subjected to high-temperature treatment in an H_2 atmosphere.

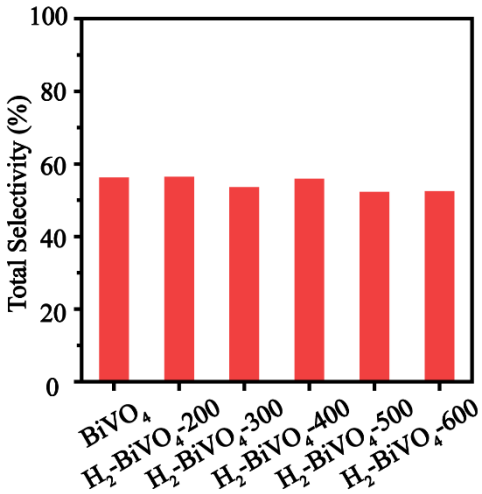

Figure S8. The product selectivity of thermal catalytic selective oxidation of benzylic C–H of toluene over the $BiVO_4$ and H_2-$BiVO_4$.

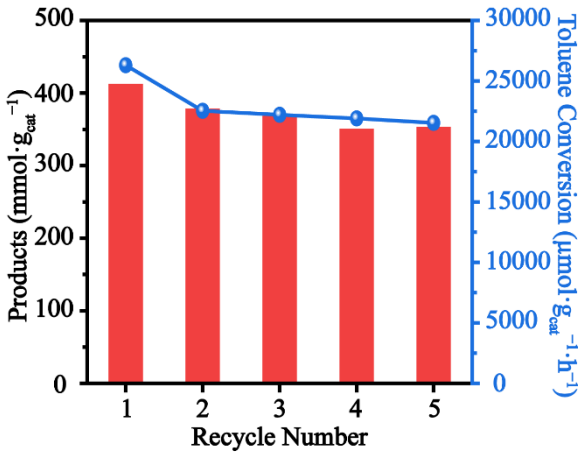

Figure S9. The stability of H_2-$BiVO_4$-300 in selective oxidation of the benzylic C–H of toluene.

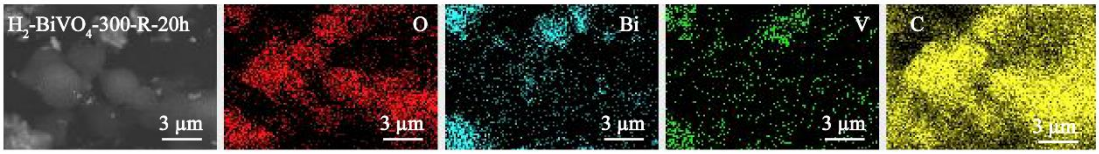

Figure S10. SEM/EDS elemental mapping of the H_2-$BiVO_4$-300-R-20h.

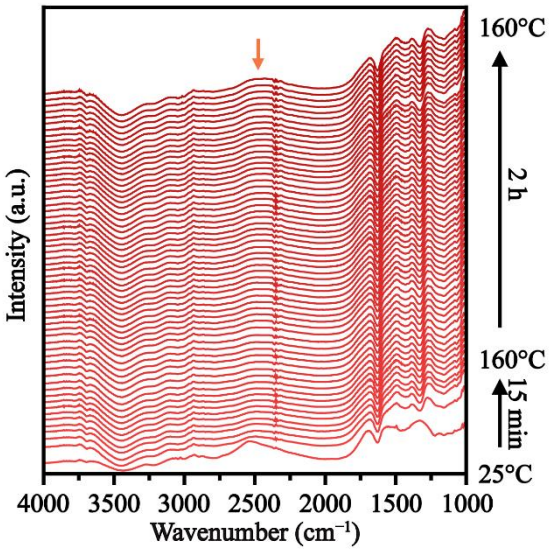

Figure S11. *In-situ* FTIR characterization of the H_2-$BiVO_4$-300 in an O_2/toluene atmosphere at 160 °C.

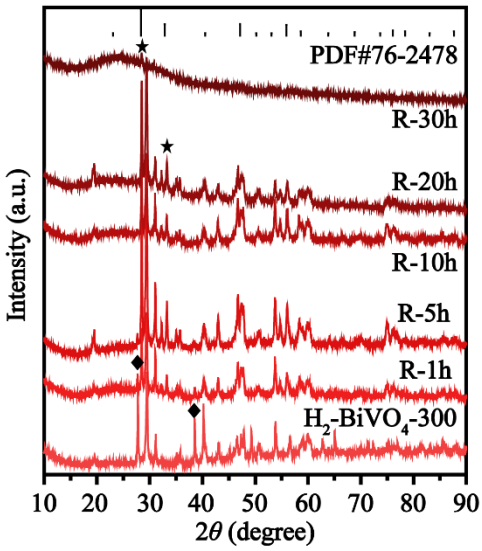

Figure S12. XRD characterization of the fresh and used H_2-$BiVO_4$-300. PDF#76-2478 is the standard card of Bi_2O_3. "R" represents the H_2-$BiVO_4$-300 after the reaction, for example, R-1h refers to the H_2-$BiVO_4$-300 after use for 1 h in the reaction. "★" is used to label the characteristic peaks belonging to Bi_2O_3. "◆" is used to label the characteristic peaks belonging to metallic Bi particle.

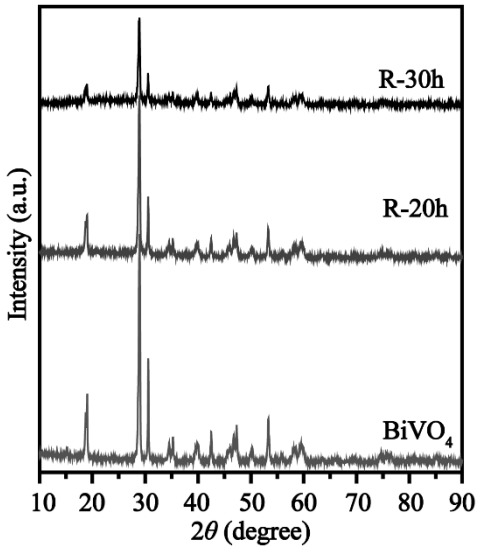

Figure S13. XRD characterization of the fresh and used $BiVO_4$. "R" represents the $BiVO_4$ after the reaction, for example, R-20h refers to the $BiVO_4$ after use for 20 h in the reaction.

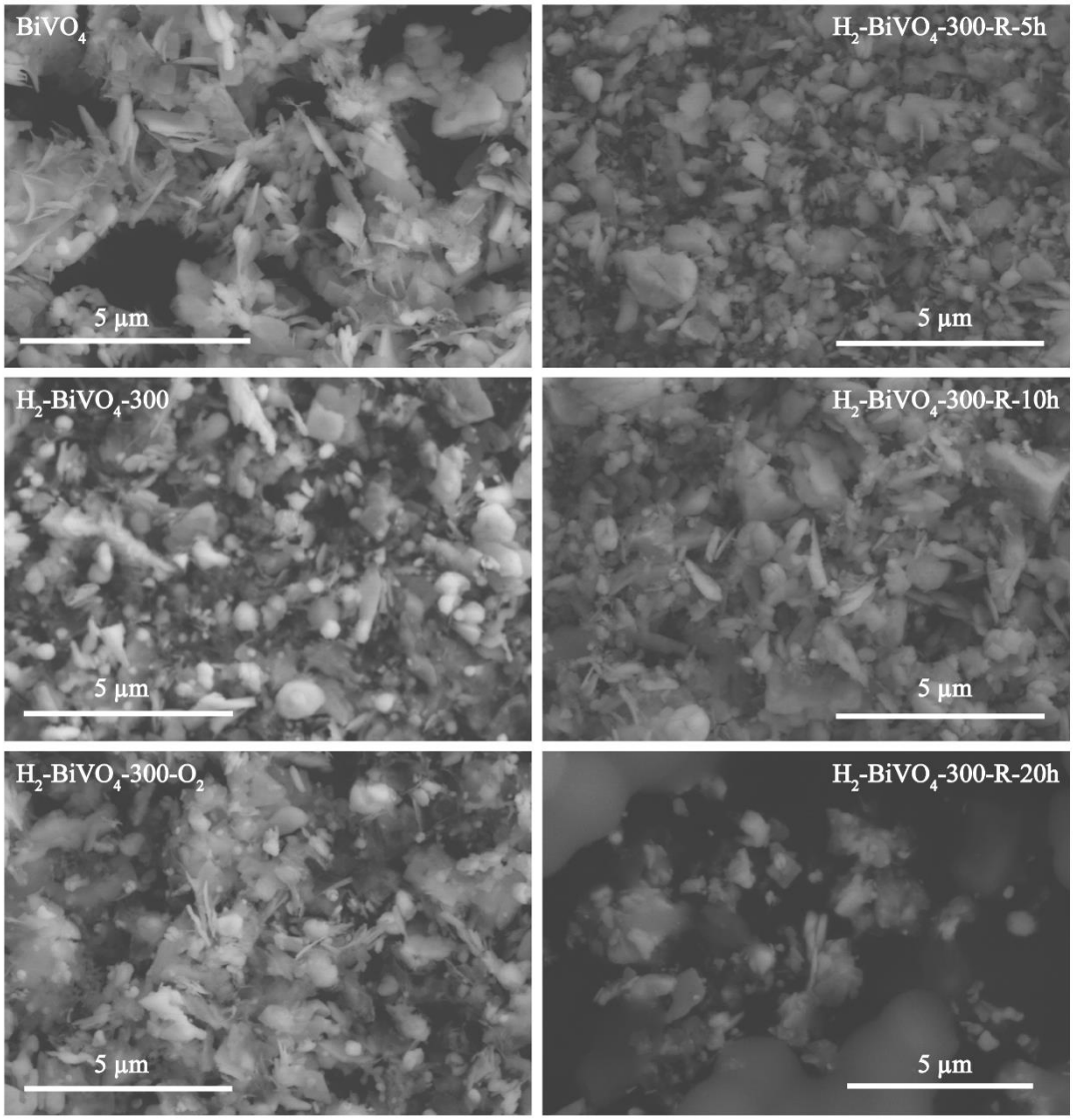

Figure S14. SEM images of the $BiVO_4$, H_2-$BiVO_4$-300, H_2-$BiVO_4$-300-O_2, H_2-$BiVO_4$-300-R-5h, H_2-$BiVO_4$-300-R-10h, and H_2-$BiVO_4$-300-R-20h.

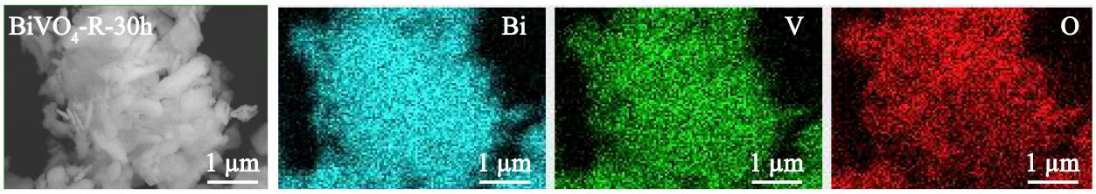

Figure S15. SEM image and corresponding elemental mapping of the $BiVO_4$-R-30h.

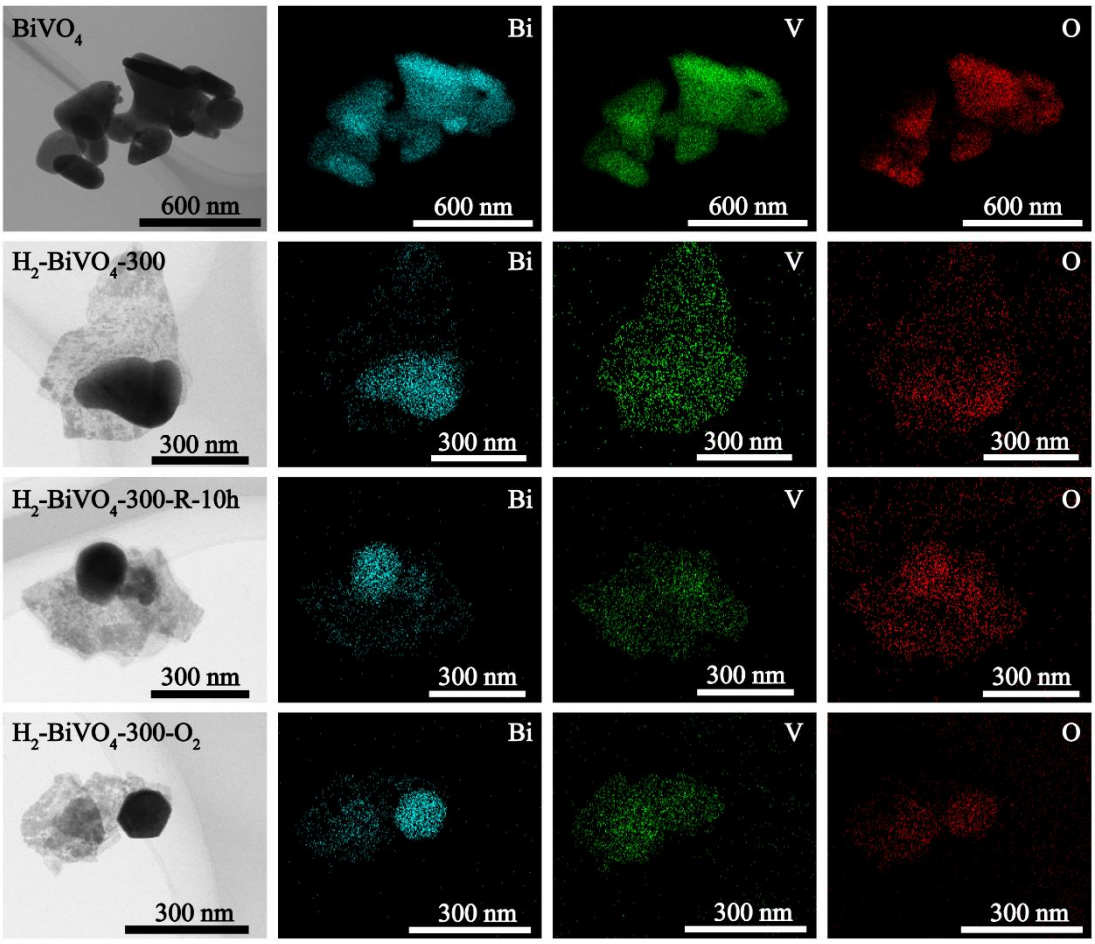

Figure S16. TEM images and the corresponding elemental mapping of the $BiVO_4$, H_2-$BiVO_4$-300, H_2-$BiVO_4$-300-R-10h, and H_2-$BiVO_4$-300-O_2.

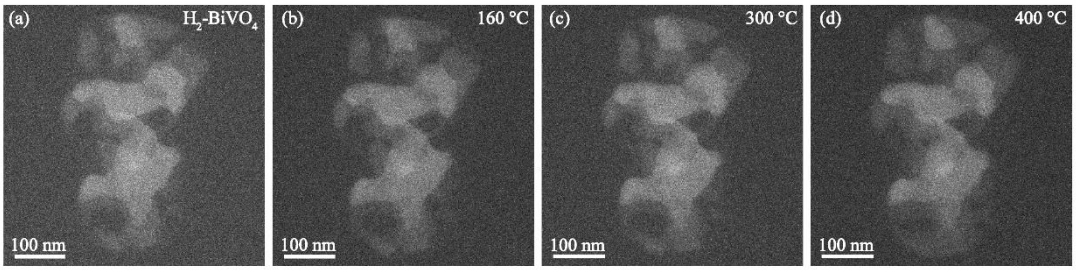

Figure S17. *In-situ* STEM images of the reduced $BiVO_4$ undergoing high-temperature reoxidation under an O_2 atmosphere.

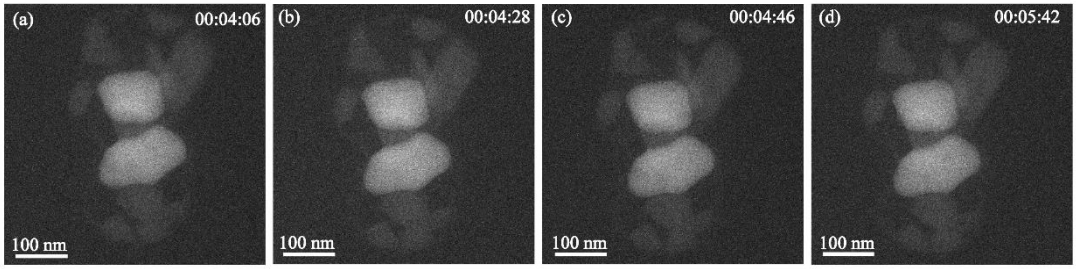

Figure S18. *In-situ* STEM images of the reduced $BiVO_4$ undergoing high-temperature reoxidation at 600 °C.

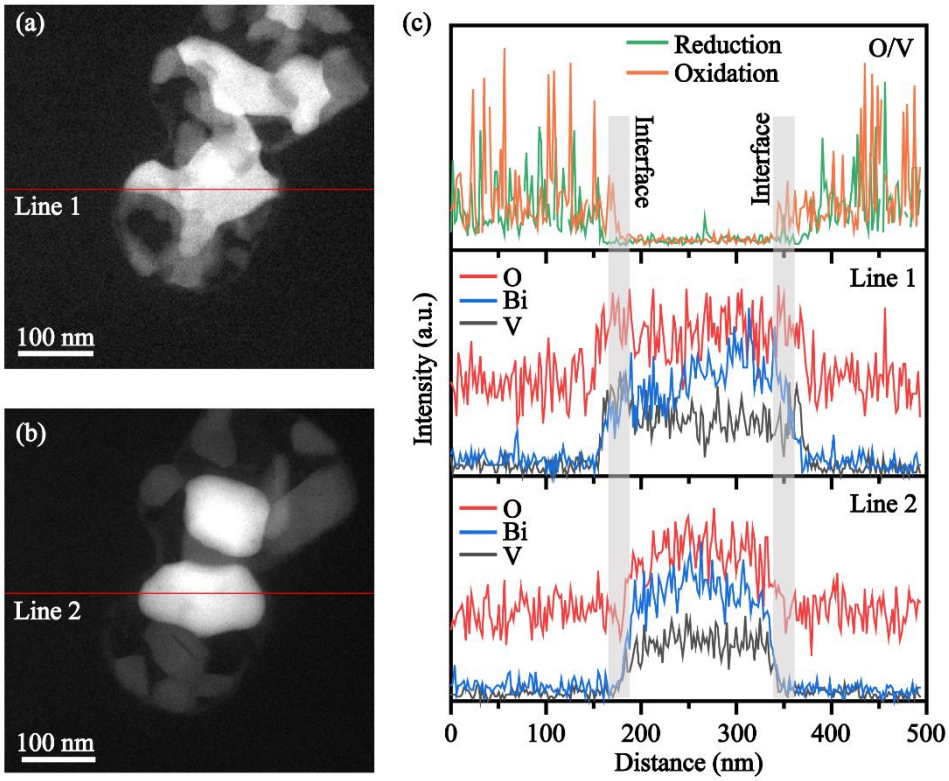

Figure S19. STEM/EDS linear scan performed on $BiVO_4$ treated with H_2 (a) and subsequently treated with O_2 (b), and the signal intensity distribution of Bi, V, and O elements and O/V intensity ratio at the corresponding linear scans (c).

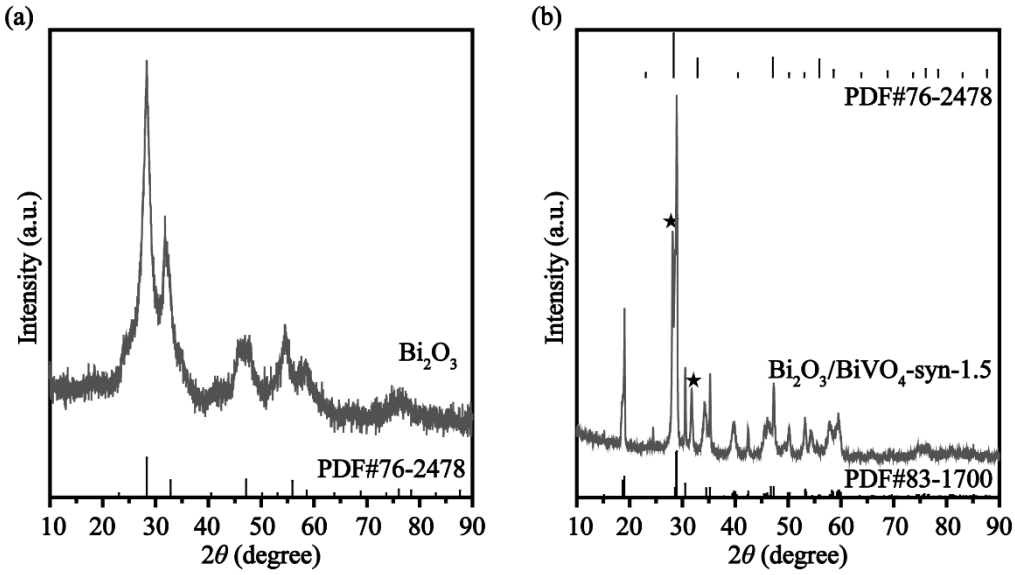

Figure S20. XRD characterization of Bi_2O_3 and $Bi_2O_3/BiVO_4$-syn-1.5. PDF#76-2478 is the standard card of Bi_2O_3. PDF#83-1700 is the standard card of $BiVO_4$. "★" is used to label the characteristic peaks belonging to Bi_2O_3.

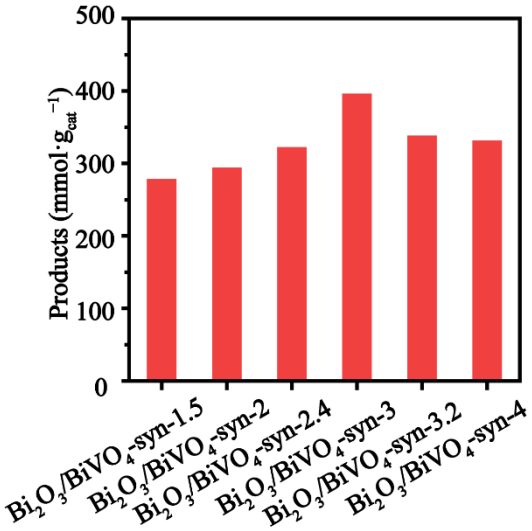

Figure S21. Thermal catalytic selective oxidation of benzylic C–H. Product yield obtained over the $Bi_2O_3/BiVO_4$-syn.

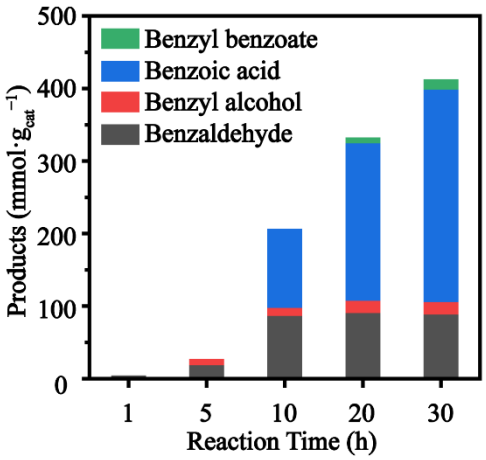

Figure S22. The yields of benzyl alcohol, benzaldehyde, benzoic acid, and benzyl benzoate obtained over H_2-$BiVO_4$-300 at different reaction time.

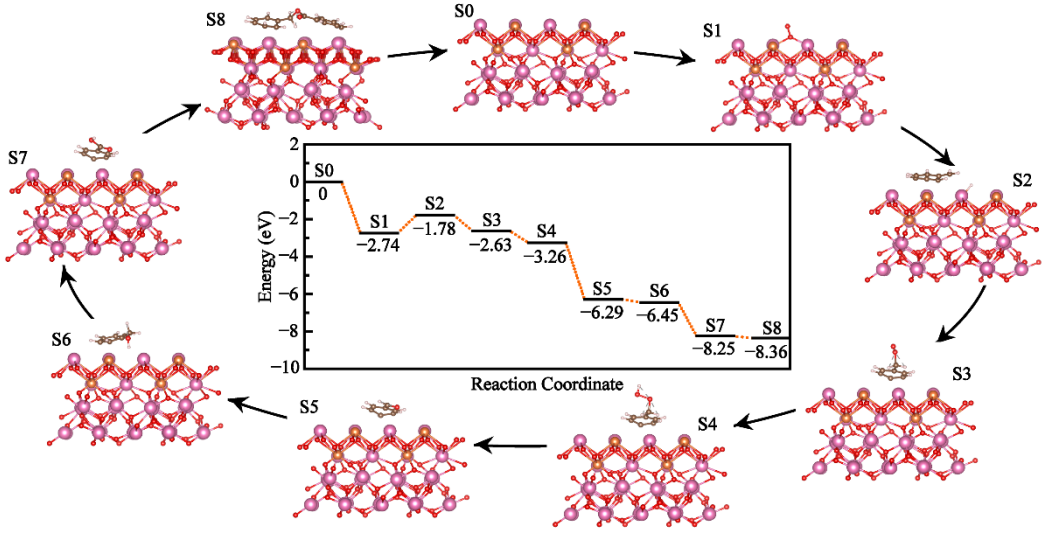

Figure S23. Reaction pathway and free-energy diagrams for generation of the high value-added products of toluene.

S1: $O_2 + e^- \rightarrow \bullet O_2^-$

S2: $C_6H_5CH_3 + h^+ \rightarrow C_6H_5CH_2\bullet + H^+$

S3: $C_6H_5CH_2\bullet + \bullet O_2^- \rightarrow C_6H_5CH_2OO\bullet^-$

S4: $C_6H_5CH_2OO\bullet^- + H^+ \rightarrow C_6H_5CH_2OOH$

S5: $C_6H_5CH_2OOH \rightarrow C_6H_5CHO + H_2O$

S6: $2\ C_6H_5CH_2OOH \rightarrow 2\ C_6H_5CH_2OH + O_2$

S7: $C_6H_5CHO + h^+ \rightarrow C_6H_5CO\bullet + H^+$

$C_6H_5CO\bullet + H^+ + 1/2\ \bullet O_2^- \rightarrow C_6H_5COOH$

S8: $C_6H_5COOH + C_6H_5CH_2OH \rightarrow C_6H_5CH_2OCOC_6H_5 + H_2O$

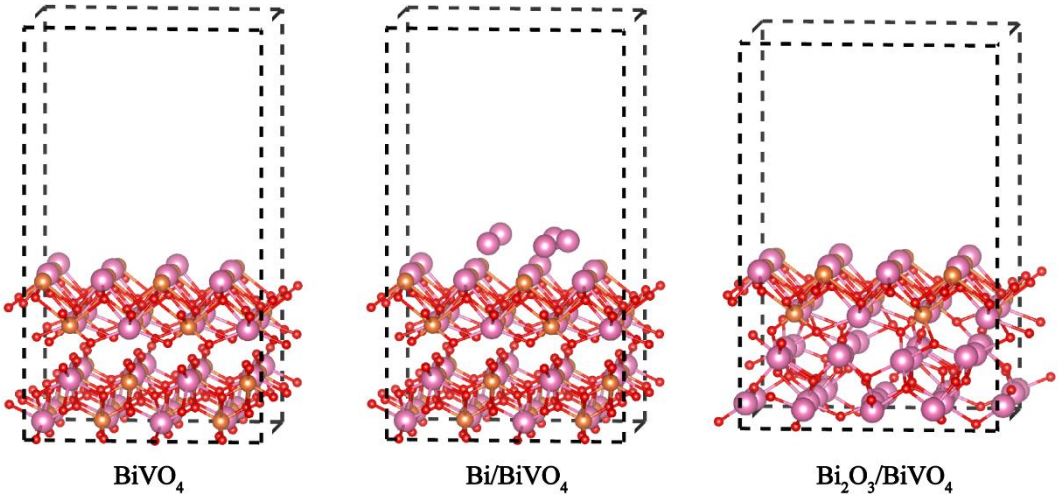

Figure S24. Optimized geometric structures of the $BiVO_4$, $Bi/BiVO_4$, and $Bi_2O_3/BiVO_4$. Pink, Bi; Orange, V; Red, O.

Table S1. The catalytic performance of $BiVO_4$-based catalysts for selective oxidation of benzylic C–H of toluene.

Catalysts	Selectivity (%)				Products ($mmol \cdot g_{cat}^{-1}$)	Toluene Conversion ($\mu mol \cdot g^{-1} \cdot h^{-1}$)	Total Selectivity (%)
	Benzaldehyde	Benzyl alcohol	Benzoic acid	Benzyl benzoate			
$BiVO_4$	38.46	11.54	5.77	0.00	29.00	1733.33	55.77
H_2-$BiVO_4$-200	13.60	6.80	34.17	1.43	309.00	18633.33	55.99
H_2-$BiVO_4$-300	11.53	2.15	37.14	2.28	410.00	26300.00	53.11
H_2-$BiVO_4$-400	13.03	2.10	38.38	1.96	389.00	23800.00	55.46
H_2-$BiVO_4$-500	12.92	1.97	35.25	1.69	363.00	23733.33	51.83
H_2-$BiVO_4$-600	13.85	2.92	33.69	1.54	333.00	21666.67	52.00
H_2-$BiVO_4$-300-HNO_3	13.88	4.13	35.37	0.99	326.00	20166.67	54.37
Bi_2O_3	15.43	16.98	21.60	1.85	178.00	10800.00	55.86
Bi_2O_3+$BiVO_4$	21.65	13.06	23.37	0.00	169.00	9700.00	58.08
Bi_2O_3/$BiVO_4$-syn-1.5	16.92	7.69	36.04	0.00	276.00	15166.67	60.65
Bi_2O_3/$BiVO_4$-syn-3	12.04	4.82	38.24	1.42	394.00	23533.33	56.62
H_2-$BiVO_4$-300-O_2	11.34	2.14	37.91	2.02	416.00	26466.67	53.40

Products = Yield (Benzyl alcohol) + Yield (Benzaldehyde) + Yield (Benzoic acid) + Yield (Benzyl benzoate);
Toluene conversion = Amount of toluene converted/(Reaction time * Catalyst dosage);
Selectivity (Benzyl alcohol) = Yield (Benzyl alcohol) / Amount of toluene converted;
Selectivity (Benzaldehyde) = Yield (Benzaldehyde) / Amount of toluene converted;
Selectivity (Benzoic acid) = Yield (Benzoic acid) / Amount of toluene converted;
Selectivity (Benzyl benzoate) = 2 * Yield (Benzyl benzoate) / Amount of toluene converted;
Total selectivity = Selectivity (Benzyl alcohol) + Selectivity (Benzaldehyde) + Selectivity (Benzoic acid) + Selectivity (Benzyl benzoate).

Table S2. Comparison of the the selective oxidation properties of benzylic C–H of toluene with the catalysts reported in the literatures.

Catalyst	Solvent	Product Yield ($mmol \cdot g_{cat}^{-1}$)	Toluene Conversion ($\mu mol \cdot g^{-1} \cdot h^{-1}$)	Reference
H_2-$BiVO_4$-300	No	410.00	26300.00	This Work
$La_2Mn_2O_6$	No	134.00	5433.33	1
N-TiO_2	No	132.80	5693.33	2
Au-Pd/TiO_2	No	59.50	2375.82	3
α-MnO_2	No	32.10	4968.53	4
mpg-C_3N_4	No	29.40	1833.62	5
Cu/Al_2O_3	No	11.60	5875.00	6
Fe_2O_3/HZSM-5	No	17.50	4952.13	7
Pd/ZSM-5	No	63.00	10750.00	8
$Co(OH)_2$/Cr_2O_3	No	101.98	10197.53	9
CrS-1	Acetic acid	10.80	830.00	10
Co_4Al oxide	Acetonitrile	4.50	989.47	11
Cu/graphene	Methanol	25.00	3120.25	12
Cu-CNB	Acetonitrile	21.00	1312.50	13
$CuCr_2O_4$	Acetonitrile	79.50	8320.67	14
Pd/C	Dimethylacetamide	2.82	61.13	15
$[n\text{-}Bu_4N]_3H_3[PW_9V_3O_{40}]$	Acetonitrile	79.00	13166.67	16

References

1. Chen, C.; Wu, M.; Chen, B.; Ma, C.; Song, M.; Jiang, G. Triggering photocatalytic performance of $La_2Co_xMn_{2-x}O_6$ via heat activation. *Proceedings of the National Academy of Sciences* **2023**, 120, e2310004120.
2. Chen, C.; Wu, M.; Yang, C.; Yu, X.; Yu, J.; Yin, H.; Li, G.; Su, G.; Hao, Z.; Song, M.; Ma, C. Electron-donating N^{-}–Ti^{3+}–O_v interfacial sites with high selectivity for the oxidation of primary C–H bonds. *Cell Reports Physical Science* **2022**, 3, 100936.
3. Kesavan, L.; Tiruvalam, R.; Rahim, M. H. A.; Saiman, M. I. B.; Enache, D. I.; Jenkins, R. L.; Dimitratos, N.; Lopez-Sanchez, J. A.; Taylor, S. H.; Knight, D. W.; Kiely, C. J.; Hutchings, G. J. Solvent-free oxidation of primary carbon-hydrogen bands in toluene using Au-Pd alloy nanoparticles. *Science* **2011**, 331, 195–199.
4. Jiang, F.; Zhu, X. W.; Fu, B. S.; Huang, J. J.; Xiao, G. M. Au/γ-MnO_2 catalyst for solvent-free toluene oxidation with oxygen. *Chinese Journal of Catalysis* **2013**, 34, 1683–1689.
5. Li, X. H.; Wang, X. C.; Antonietti, M. Solvent-free and metal-free oxidation of toluene using O_2 and g-C_3N_4 with nanopores: Nanostructure boosts the catalytic. *ACS Catalysis* **2012**, 2, 2082–2086.
6. Wang, F.; Xu, J.; Li, X.; Gao, J.; Zhou, L.; Ohnishi, R. Liquid phase oxidation of toluene to benzaldehyde with molecular oxygen over copper-based heterogeneous catalysts. *Advanced Synthesis & Catalysis* **2005**, 347, 1987–1992.
7. Li, X.; Lu, B.; Sun, J.; Wang, X.; Zhao, J.; Cai, Q. Selective solvent-free oxidation of toluene to benzaldehyde over zeolite supported iron. *Catalysis Communications* **2013**, 39, 115–118.
8. Fu, B.; Zhu, X.; Xiao, G. Solvent-free selective aerobic oxidation of toluene by ultra fine nano-palladium catalyst. *Applied Catalysis A: General* **2012**, 415, 47–52.
9. Miao, S.; Wang, F.; Liu, J.; Mao, W.; Yin, B.; Li, Y. Solvent-free toluene aerobic selective oxidation over $Co(OH)_2/Cr_2O_3$: The effect of calcination temperature on product selectivity. *Applied Catalysis A: General* **2022**, 643, 118787.
10. Singh, A. P.; Selvam, T. Liquid phase oxidation reactions over chromium silicalite-1 (CrS-1) molecular sieves. *Journal of Molecular Catalysis A: Chemical* **1996**, 113, 489–497.
11. Zhou, W.; Huang, K.; Cao, M.; Sun, F.; He, M.; Chen, Z. Selective oxidation of toluene to benzaldehyde in liquid phase over CoAl oxides prepared from hydrotalcite-like precursors. *Reaction Kinetics, Mechanisms and Catalysis* **2015**, 115, 341–353.
12. Song, G.; Feng, L.; Xu, J.; Zhu, H. Liquid-phase oxidation of toluene to benzaldehyde with molecular oxygen catalyzed by copper nanoparticles supported on graphene. *Research on Chemical Intermediates* **2018**, 44, 4989–4998.
13. Han, H.; Ding, G.; Wu, T.; Yang, D.; Jiang, T.; Han, B. Cu and boron doped carbon nitride for highly selective oxidation of toluene to benzaldehyde. *Molecules* **2015**, 20, 12686–12697.
14. Acharyya, S. S.; Ghosh, S.; Tiwari, R.; Sarkar, B.; Singha, R. K.; Pendem, C.; Sasaki, T.; Bal, R. Preparation of the $CuCr_2O_4$ spinel nanoparticles catalyst for selective oxidation of toluene to benzaldehyde. *Green Chemistry* **2014**, 16, 2500–2508.
15. Zhang, J.; Du, J.; Zhang, C.; Liu, K.; Yu, F.; Yuan, Y.; Duan, B.; Liu, R. Selective oxidation of alkylarenes to the aromatic ketones or benzaldehydes with water. *Organic Letters* **2022**, 24, 1152–1157.
16. Ma, B.; Zhang, Z.; Song, W.; Xue, X.; Yu, Y.; Zhao, Z.; Ding, Y. Solvent-free selective

oxidation of C–H bonds of toluene and substituted toluene to aldehydes by vanadium-substituted polyoxometalate catalyst. *Journal of Molecular Catalysis A: Chemical* **2013**, 368, 152–158.